

## INTERSTELLAR COMMUNICATION. I. MAXIMIZED DATA RATE FOR LIGHTWEIGHT SPACE-PROBES

MICHAEL HIPPKÉ<sup>1</sup><sup>1</sup>*Sonneberg Observatory, Sternwartestr. 32, 96515 Sonneberg, Germany*

## ABSTRACT

Recent technological advances could make interstellar travel possible, using ultra-lightweight sails pushed by lasers or solar photon pressure, at speeds of a few percent the speed of light. Obtaining remote observational data from such probes is not trivial because of their minimal instrumentation (gram scale) and large distances (pc). We derive the optimal communication scheme to maximize the data rate between a remote probe and home-base. The framework requires coronagraphic suppression of the stellar background at the level of  $10^{-9}$  within a few tenths of an arcsecond of the bright star. Our work includes models for the loss of photons from diffraction, technological limitations, interstellar extinction, and atmospheric transmission. Major noise sources are atmospheric, zodiacal, stellar and instrumental. We examine the maximum capacity using the “Holevo bound” which gives an upper limit to the amount of information (bits) that can be encoded through a quantum state (photons), which is a few bits per photon for optimistic signal and noise levels. This allows for data rates of order bits per second per Watt from a transmitter of size 1 m at a distance of  $\alpha$  Centauri (1.3 pc) to an earth-based large receiving telescope (E-ELT, 39 m). The optimal wavelength for this distance is 300 nm (space-based receiver) to 400 nm (earth-based) and increases with distance, due to extinction, to a maximum of  $\approx 3 \mu\text{m}$  to the center of the galaxy at 8 kpc.

## 1. INTRODUCTION

Interstellar travel became technologically plausible in the 1950s, when the energy release of thermonuclear fusion was observed in the first hydrogen bombs. First studies were based on the idea of a pulse drive, directly propelled by the explosions of atomic bombs behind the craft (Dyson 1965, 1968), evolving into a direct fusion rocket (Bond & Martin 1978). These designs were manned interstellar arks with masses of order 10 million tonnes and speeds of 10% the speed of light.

Classical rockets, both chemical and nuclear, suffer from the limitations imposed by Tsiolkovsky’s rocket equation (Plastino & Muzzio 1992): if a rocket carries its own fuel, the ratio of total rocket mass versus final velocity is an exponential function, making high speeds extremely expensive. A different method, which does not require the fuel to be accelerated with the ship, has been proposed by Johannes Kepler (1604). After observing a comet, he suggested that the cometary tail points away from the sun due to a “breeze”, and proposed to “provide ships or sails adapted to the heavenly breezes, and there will be some who will brave even that void.”. James Clerk Maxwell predicted that radiation carries momentum and exerts pressure: “Hence in a Medium in which waves are propagated there is a pressure in the direction normal to the wave, and numerically equal to

the energy in unit of volume” (Maxwell 1873; Maxwell & Harman 1990).

Redding (1967) noted that there was no obvious way to decelerate the spacecraft at the target star system. Only recently, Heller & Hippke (2017) and Heller et al. (2017) suggested to decelerate using the stellar radiation and gravitation in a maneuver they referred to as photogravitational assist. A project by the “Breakthrough Initiatives”<sup>1</sup> provides monetary support (of order 100 m USD) for research on gram-scale robotic spacecrafts, using a light sail for propulsion (Lubin 2016; Popkin 2017).

Between “Project Orion”, and the “nanocraft concept”, there is a factor of  $10^{13}$  in weight. The smaller weight results in lower build- and launch costs, a benefit that could make such a mission affordable within the current century. When we compare the early studies with the most recent concept, we have to distinguish that the main purpose of interstellar travel shifted from colonization of exoplanets with human (biological) settlers to unmanned research probes, taking spectroscopic and photographic measurements of the putative biological environment on potentially habitable exoplanets. Software and hardware engineering has made sufficient progress since the 1960s that such probes can be highly autonomous. Consequently, the required mass for probes can be reduced.

Our benefit from autonomous interstellar probes is purely in the information they send back to us. Thus we shall seek to maximize the amount of information we can obtain from them. A major issue is that these probes are designed to be very light-weight, and thus limited in terms of power. While traditional, fusion-based concepts proposed the use of high (MW, [Milne et al. 2016](#)) power at GHz frequencies for data transfer, small sailing probes can not have a fusion reactor on board and will have to rely on photovoltaic energy, which delivers of order kW per square meter surface area. In the current era of high resolution video, a high data rate to transfer spectacular observations of an alien world could be important for the public reception of such a mission, and thus its financial funding. It is therefore crucial to optimize interstellar communication, precisely the data rate, to maximize the data volume of scientific and public data.

In this work, paper I of the series, our contributions are: (1) to introduce the variables in the framework of data transfer between telescopes; (2) to assess limiting factors such as extinction, noise, and technological constraints; and (3) to calculate optimal frequencies and achievable data rates for exemplary cases.

## 2. METHOD TO CALCULATE DATA RATES

The free-space photon flux  $F$  received from a telescope at distance  $d$  can be calculated as ([Kaushal et al. 2017](#)):

$$F = \frac{P_t}{\pi h f (\theta d)^2} \quad (1)$$

where  $P_t$  is the transmitted power,  $f$  the photon frequency, and  $h$  Planck's constant ( $\approx 6.626 \times 10^{-34}$  Js). The (half) opening angle of the diverging light beam is  $\theta_d = Q_R \lambda / D_t$  (in radians) with  $Q_R \approx 1.22$  for a diffraction limited circular transmitting telescope of diameter  $D_t$  ([Rayleigh 1879](#)), and  $\lambda = c/f$  with  $c$  as the speed of light in vacuum ( $299,792,458 \text{ m s}^{-1}$ ). In a receiving telescope with aperture  $A_R = \pi D_r^2/4$  we obtain the flux

$$\begin{aligned} F_r &= \frac{P_t}{\pi h f (Q_d \lambda / D_t)^2 d^2} \times \frac{\pi D_r^2}{4} \\ &= \frac{P_t D_t^2 D_r^2}{4 h f Q_d^2 \lambda^2 d^2} (\text{s}^{-1}). \end{aligned} \quad (2)$$

This assumes a uniform plane-wave illumination. A telescope with central obscuration and plane-wave gaussian-beam illumination has been calculated by [Klein & Degnan \(1974\)](#), and the flux loss from pointing errors by [Marshall \(1987\)](#); but these secondary effects will be neglected here. For a laserbeam, the narrower ‘‘waist’’ leads to an intensity pattern with a characteristic angular beam size given by ([Duarte 2015](#); [Tellis & Marcy 2015](#))  $\theta_L = Q_L (2/\pi) \lambda / D$ , or  $\theta_L / \theta_d \approx 0.5$ , which leads to a tightening of the beam. Note that a laserbeam shape is not maintained in systems where laser light is

broadened with a beam expander and then focused with a telescope, and so we neglect this possibility here.

The widely used approximation<sup>2</sup> of the diffraction-limited aperture,  $\theta \approx \lambda/D$ , leads to an overestimate of the received photon flux on the receiver side by  $\approx 49\%$ . This can be verified by setting  $Q_R = 1$  versus  $Q_R = 1.22$  numerically. The considerable difference comes from the fact that  $\theta$  enters the equation through the inverse square law. The precise value,  $\theta = 1.2196 \dots \lambda/D$  comes from the Fraunhofer diffraction where this number is the first zero of the order-one Bessel function of the first kind,  $J_1(x)/\pi$ .

Several factors will constrain the achievable data rates. Regarding the loss of photons, the most important are interstellar extinction (section 3.1), of which we denote the surviving fraction as  $0 < S_E < 1$ . For ground-based telescopes, atmospheric transmission allows for the reception of another fraction of photons,  $0 < S_A < 1$  (section 3.2). The receiver efficiency is denoted as  $0 < \eta < 1$ . Technological constraints on the telescopes will be denoted as  $Q$  (section 3.3). Other small factors, such as scintillation and scattering (section 4.4), might play a role and can be included in calculations in a similar manner, but we neglect them here for brevity. The major noise sources are atmospheric sky background (section 4.1), zodiacal light (section 4.2), and others (sections 4.5, 4.6).

### 2.1. Channel capacity for a coherent wave

We now define the theoretical maximum data rates based on frequency, signal and noise. For completeness, we will first discuss the optimum case where the number of photons received is sufficiently large to form a coherent wave. While this might not be realistic for most schemes of interstellar communication (section 5), it is useful to define the classical upper bound. The maximum rate at which information can be transmitted over a communications channel is ([Shannon 1949](#)):

$$C = B \log_2 \left( 1 + \frac{S}{N} \right) \quad (3)$$

where  $C$  is the channel capacity (in bits per second),  $B$  is the bandwidth of the channel (in Hertz),  $S$  is the average signal power (in Watt) and  $N$  is the average gaussian noise (in Watt). The bandwidth is the difference between the highest ( $f_H$ ) and lowest ( $f_L$ ) frequency in a continuous set of frequencies.

To compare data rates for different frequencies, we can approximate bandwidth with frequency by taking a constant fractional bandwidth,  $b$ . With  $f_C$  as the center frequency, we can define  $b = (f_H - f_L)/f_C$ . With a value of e.g.  $b = 0.1$ , we can approximate  $B \approx c/\lambda$  (in Hz).

<sup>2</sup> Approximations and mistakes in the literature will be discussed in section 6.8.

Channel capacity is proportional to frequency and to the logarithm of S/N. These relations suggest that the frequency should be increased to the practical maximum, and that the signal power should merely be increased to overcome noise, with little benefit beyond.

If the received number of photons (after extinction and other losses) is sufficiently large to form a coherent wave, we can plug Eq. 2 (as the signal  $S$  in photons per second) into 3, and define the noise equally in photons per second:

$$\text{DSR}_c = \frac{c}{\lambda} \log_2 \left( 1 + \frac{F_r}{N_\gamma} \right) \quad (4)$$

where  $N_\gamma$  is the number of photons ( $\gamma$ ) from noise per second (physical and instrumental). Then, the data signaling rate for the case of a continuous wave,  $\text{DSR}_c$ , can be conveniently calculated in units of bits/s if  $P$  is in Watt.

Intuitively, one would assume that at least one photon is required to transfer one bit of information, but this is incorrect: More than one bit can be encoded per photon. This is done with a modulation scheme to define an alphabet, often using a combination of polarization, phase, frequency and amplitude modulation (e.g., Jones 1995). Each symbol of such an alphabet can encode several bits, scaling with the logarithm to base 2 of the number of members. This is called spectral efficiency and is measured in (bits/s)/Hz. Modulation rate, spectral efficiency and data rate can be increased for a constant bandwidth at the cost of an exponential rise in SNR, or, for a constant noise level, in an exponential increase in  $P$ .

For the extreme case of communication with negligible losses (e.g.,  $d \rightarrow 0$ ), Eq. 3 suggests the use of infinitely high bandwidth. However, infinite frequencies (and infinite capacity) are unphysical. In the classical sense, the limit comes from the fact that an increase in bandwidth also increases noise power (Shannon's power efficiency limit). A noiseless channel has infinite capacity: with Eq. 3 we have  $C = B \log_2(1 + \infty) = \infty$ . However, in reality noise is never zero because photons are quantized (section 4.6). Then, the capacity of Shannon's limit becomes (Chitode 2009, p. 5-117):

$$\lim_{B \rightarrow \infty} C = \frac{S}{N} \log_e 2 \approx 1.44 \frac{S}{N} \quad (5)$$

In the framework of quantum state propagation, any transmission system can exchange only a limited (quantized) amount of information in a given time frame (Yuen & Shapiro 1978), and is thus limited by physical resources (Bekenstein 1981). Therefore, increasing frequency to infinity does not increase data rate to infinity (Giovannetti et al. 2004b).

## 2.2. The photon limited case

The limit for Eq. 3 only applies if the number of photons is sufficiently large to form a coherent wave.

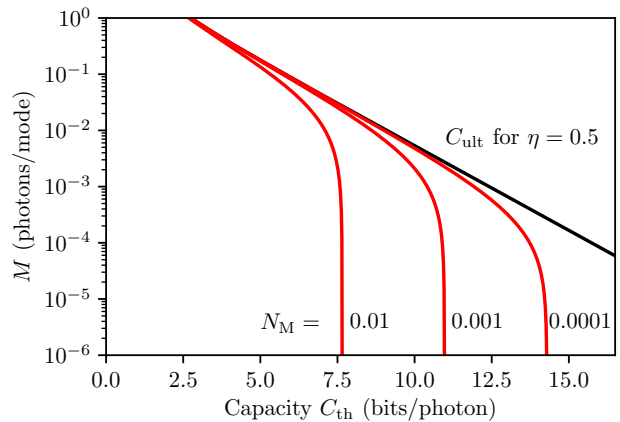


**Figure 1.** Capacity  $C_{th}$  in bits per photon as a function of the number of photons per mode,  $M$ . The larger the number of modes, the more bits can be encoded per photon, however the ultimate bound (black) is logarithmic. When accounting for thermal noise per mode  $N_M$  (fractions in the plot), the limits are even tighter (red lines).

In many schemes for interstellar communication (section 5), the data rate is photon-limited. Then, Holevo's bound (Holevo 1973) establishes the upper limit to the amount of information which can be transmitted with a quantum state. It applies independently from the frequency of the wave, and assumes that a number (quantity) of modes can be used per photon, which originate from the photons' dimensions, namely polarization, frequency and time of arrival. The inverse of this quantity,  $M$ , is the number of photons per mode. Then, as shown by Giovannetti et al. (2004b), the ultimate quantum limit of bits per photon can be expressed as:

$$C_{ult} = g(\eta M) \quad (6)$$

where  $\eta$  is the receiver efficiency and  $g(x) = (1 + x) \log_2(1 + x) - x \log_2 x$  so that  $g(x)$  is a function<sup>3</sup> of  $\eta \times M$ . In the presence of thermal noise, it was conjectured (Giovannetti et al. 2004a) and recently proven (Giovannetti et al. 2014) that the capacity is:

$$C_{th} = g(\eta M + (1 - \eta)N_M) - g((1 - \eta)N_M) \quad (7)$$

where  $N_M$  is the average number of noise photons per mode. It is an open question if the maximum can fully, or only approximately be achieved in practice (Wilde et al. 2012; Guha & Wilde 2012). The achievable capacity is shown for a wide range of modes in Figure 1. It is clear that even large numbers of modes and small fractional noise increase the number of bits per photon only within a factor of a few.

<sup>3</sup> An introduction into quantum information theory and the usual notation can be found in Takeoka & Guha (2014).

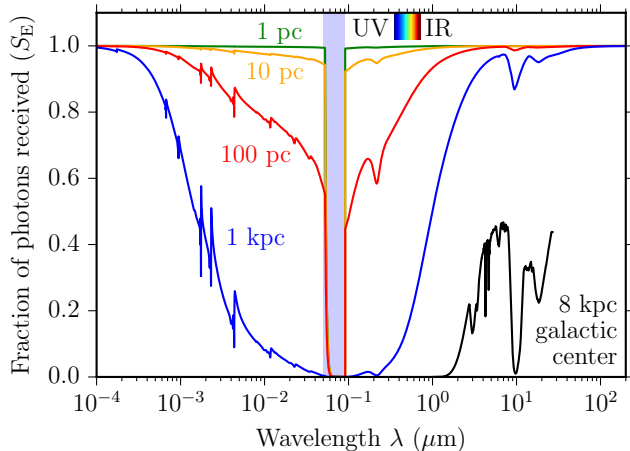


**Figure 2.** Fraction of photons that defies interstellar extinction ( $S_E$ ), as a function of wavelength  $\lambda$ , shown for different distances. The shaded area represents the Lyman continuum ( $\approx 50 - 91.2$  nm) which is opaque even for the closest stars due to the ionization of neutral hydrogen (Aller 1959; Wilms et al. 2000; Barstow & Holberg 2007).

We can multiply Eq. 2 and Eq. 7 to calculate the data rate for the photon limited case of two communicating telescopes:

$$\text{DSR}_\gamma = C_{\text{th}} F_r \quad (8)$$

where  $\text{DSR}_\gamma$  is in units of bits/s when  $P$  is in Watt. It assumes that the free path loss caused by  $\eta, d, S_E, S_A$  is known and accounted for in the encoding scheme. Variations and uncertainties in the number of received photons can be treated as an additional noise source, but optimal encoding schemes will be neglected in this paper. In the following sections, we will discuss the values in these equations.

### 3. SIGNAL LOSSES

#### 3.1. Loss of photons from extinction

From the IR to the UV, extinction is caused by the scattering of radiation by dust, while at wavelengths shorter than the Lyman limit (91.2 nm), extinction is dominated by photo-ionisation of atoms (Ryter 1996). For short interstellar distances, extinction in the optical is small,  $\approx 0.1$  mag within 100 pc, 0.05–0.15 mag out to 200 pc (Vergely et al. 1998). It is much larger towards the galactic center,  $E(B - V) \approx 3$  at  $A(V) > 44$  mag at 550 nm (Porquet et al. 2008; Fritz et al. 2011), an attenuation by a factor of  $10^{-18}$ . Another prominent feature in measured extinction curves is a “bump” in the UV at 217.5 nm (Stecher 1965, 1969), where extinction is about an order of magnitude higher. It is attributed to organic carbon and amorphous silicates present in the grains (Bradley et al. 2005). Other features are the water ice absorption at  $3.1 \mu\text{m}$  and the 10 and  $18 \mu\text{m}$  silicate absorption.

While higher frequencies have higher channel capacities for coherent waves, and allow for tighter beams (at a given telescope size), they also generally suffer from higher extinction between UV and IR. To analyze this trade-off (section 5.6), we use the synthetic extinction curve presented in Draine (2003a,b,c) which covers wavelengths from 1 cm (30 GHz) to  $1 \text{ \AA}$  (12.4 keV). We scale this curve for different distances using  $A(V) = 1.8$  mag per kpc in the galactic plane (Whittet 2003), equivalent to  $E(B - V) = 0.28$  mag per kpc (Dias et al. 2002). For the highest extinction values towards the galactic center, where  $E(B - V) \approx 3$ , we use measurements for the optical and IR (Fritz et al. 2011) and the UV (Valencic et al. 2004; McJunkin et al. 2016) and interpolate in between individual data points with a spline. This extinction curves covers the wavelength range from  $0.1 - 27 \mu\text{m}$ . While extinction is typically given in astronomical magnitudes, we convert these to the fraction of photons received over distance ( $S_E$ ), and show examples in Figure 2.

#### 3.2. Loss of photons from atmospheric transmission

The earth is surrounded by an atmosphere (Forbes 1842), which is essential for almost all life on this planet (Canfield et al. 2007), but of the greatest annoyance for almost all astronomers (Kuiper 1950). For a space telescope there is no loss of photons from a surrounding cloud of gas, dust and water, so that the surviving fractions of photons is  $S_A = 1$ . On earth, atmospheric transmission depends on the wavelength and varying characteristics, such as the content of water vapor in the air. As an example, we use a transmission curve  $S_A(\lambda)$  for Mauna Kea with a water vapor column of 1 mm, which represents excellent observing conditions, and occurs in the 20% of the best nights of an average year (Lord 1992; Guharay et al. 2009). This curve covers the wavelength range of 200 nm–10 cm (3 GHz). Figure 3 shows the part up to 10 mm (30 GHz), after which transmission reaches near unity.

Transmission is zero for all practical purposes for wavelengths below 291 nm, above 20 m, and between  $30 - 200 \mu\text{m}$ . In the optical and infrared, transmission is highly variable due to numerous absorption lines from water, carbon dioxide, ozone and other gases. When communicating with photons in a narrow (nm) bandwidth, as is common with lasers, the exact wavelength must be chosen carefully, because transmission fluctuates rapidly. For example,  $S_A = 0.98$  at  $\lambda = 934.36$  nm, but  $S_A = 0.22$  at  $\lambda = 934.52$  nm, a spectral distance of only 0.16 nm. Under good atmospheric conditions, transmission can be close to unity for many wavelengths in the optical and near- to mid-infrared.

For brevity, we neglect other atmospheric effects such as scattering and turbulence (“seeing”, Coulman et al. 1995) which is a variation of the optical refractive index and enlarges the point spread function of the telescope, if not corrected for with adaptive optics (Hardy 1998).

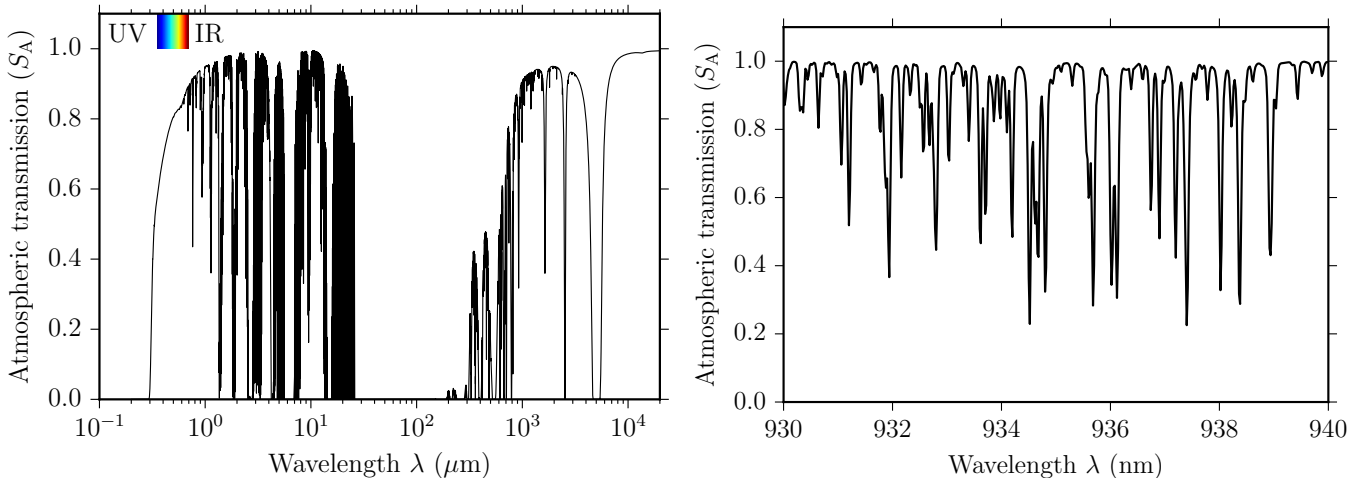


**Figure 3.** Left: Surviving fraction of photons after atmospheric transmission ( $S_A$ ) as a function of wavelength. Short-ward of UV (291 nm), transmission remains at zero. Data is for Mauna Kea in best (20-percentile) conditions. Right: Zoom into the IR with fluctuations from 0.2 to unity transmission with typical line widths of  $2 \text{ \AA} = 0.2 \text{ nm}$ .

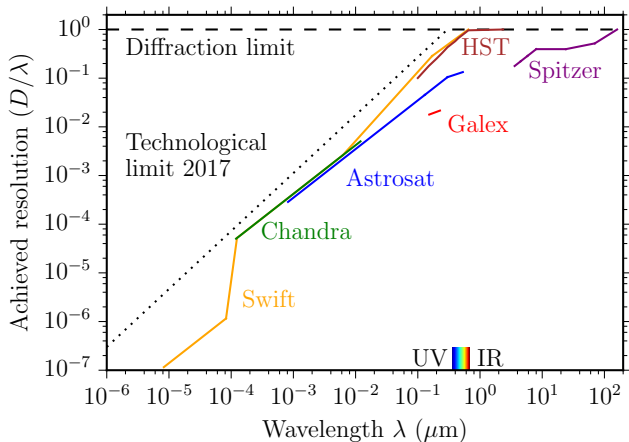


**Figure 4.** Technologically achieved resolution for space telescopes (earth 2017) as a function of wavelength. Focusing high-energy waves is increasingly difficult.

### 3.3. Technological limits of telescopes

The angular beam size is limited to  $Q_R \geq 1.22$  (Rayleigh limit), or  $Q_L \geq 1$  for a laserbeam. Technology may place a stricter limit. We have examined the angular resolution of current (earth 2017) space telescopes for different wavelengths. As can be seen in Figure 4,  $Q_{\text{real}}/Q_R$  is an exponential function for wavelengths  $\lambda < 300 \text{ nm}$ , indicating the technological difficulty to focus wavelengths in UV and shorter.

For diffraction-limited telescope mirrors, the polished surfaces need to have surface smoothness  $< \lambda/4$  (Danjon & Couder 1935), which makes the production of telescopes for UV, X-ray and  $\gamma$ -ray increasingly difficult. Additionally, the refractive index of all known materials is close to 1 at high (keV) energies, making it difficult to

focus photons efficiently and avoid absorption (Aristov & Shabel'nikov 2008).

With today's technology, resolution in the milli-arcsec regime is possible at optical wavelengths, but X-rays are limited to angular resolutions of 20 arcsec (Salmaso et al. 2014), a difference of 4 orders of magnitude. For example, the Swift X-Ray satellite has an angular resolution of 18 arcsec at  $\lambda = 1 \text{ nm}$  (1.5 keV) from a 30 cm aperture (Burrows et al. 2005), while the diffraction limit would be  $1.22\lambda/D = 8 \times 10^{-4}$  arcsec, so that  $Q_{\text{real}}/Q_R = 4 \times 10^{-5}$ . Technology is believed to eventually achieve sub-arcsec resolution at X-rays, but at the expense of large designs, with focal lengths of  $10^5 \text{ km}$  (Gorenstein 2004).

### 3.4. Technological limits of the receiver

Photon energy depends on wavelength,  $E = hc/\lambda$ , which should make it easier to detect higher energy photons in theory. In practice, single photon detection with high quantum efficiency is possible throughout a wide range of wavelengths, from X-Rays (Tanguay et al. 2013, 2015) to microwaves (Poudel et al. 2012; Wong & Vavilov 2015). Interestingly, even the human eye can detect single photons in the visible light (Tinsley et al. 2016).

We will neglect a possible wavelength-dependence in quantum efficiency of photon detectors in this paper. This is supported by the much stronger influence from technological limits in focusing beams (section 3.3), and the influence of interstellar extinction on photon throughput (section 3.1), so that detector differences (of a few percent) will be negligible for most practical cases.

## 4. NOISE

Noise sources can be astrophysical (scattering of the signal, background light) or instrumental (shot noise and read noise). For ground-based telescopes, the total noise

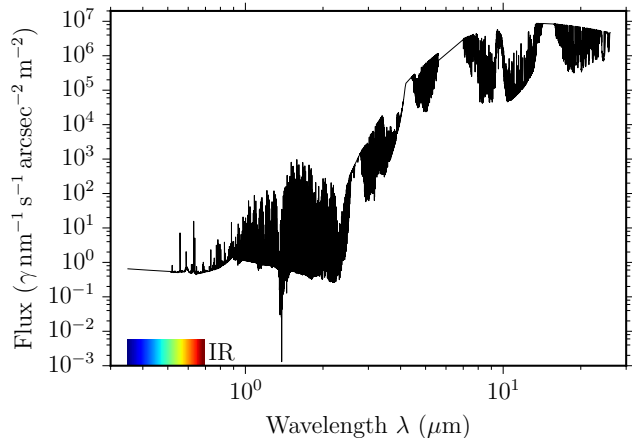


**Figure 5.** Atmospheric sky background on Mauna Kea as a function of wavelength.

has been measured (section 4.1), for space-based telescopes, it will be discussed in sections 4.2–4.6.

#### 4.1. Atmospheric sky background

For a telescope located on earth, the total sky background which enters as noise into the receiver can be measured by observing a (maximally) empty sky area. Naturally, it includes all sources: terrestrial, solar system, and interstellar.

Precise raw sky emission data is available for many observatory sites, and as in section 3.2 we use Mauna Kea as an example. The measurements are for the sky background only and do not include the emission from a telescope or sensor (which has been subtracted out). The data were manufactured with a synthetic sky transmission (Lord 1992) subtracted from unity. This gives an emissivity which is then multiplied by a blackbody function with a temperature of 273 K (Guharay et al. 2009). The authors added emission spectra based on observations from Mauna Kea, and the dark sky continuum mostly from zodiacal light. Finally, the curve has been scaled to produce 18.2 mag arcsec<sup>-2</sup> in the H band, as observed on Mauna Kea by Maihara et al. (1993). The resolution of the final data product is 0.1 nm<sup>4</sup>.

These values are in agreement with measurements from the darkest observatory sites on earth, which have an optical sky background minimum of 22 mag arcsec<sup>-2</sup> (Smith et al. 2008), corresponding to an optical flux of a few  $\gamma$  arcsec<sup>-2</sup> sec<sup>-1</sup> from unresolved sky sources, air glow, and zodiacal light.

The sky background at Mauna Kea is shown in Figure 5 and covers the band from 300 nm–30  $\mu$ m. Similarly to the transmission (section 3.2), background levels vary

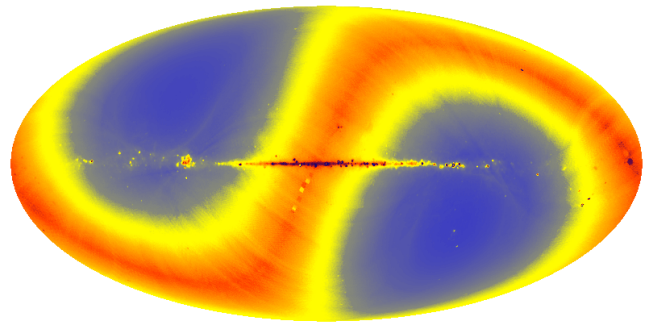


**Figure 6.** All-sky map at 12  $\mu$ m taken by the COBE satellite (Boggess et al. 1992; Kelsall et al. 1998). The horizontal line is the galactic plane, the S-shaped band represents the solar system ecliptic, where zodiacal light is  $> 100\times$  higher than near the ecliptic poles (blue colors, Levasseur-Regourd & Dumont 1980).

by up to 3 orders of magnitude over few nm. Generally, the flux is  $\approx \gamma$  nm<sup>-1</sup> arcsec<sup>-2</sup> m<sup>-2</sup> in the optical and NIR, with a steep increases for  $\lambda > 2.5 \mu$ m, and reaches  $10^7 \gamma$  nm<sup>-1</sup> arcsec<sup>-2</sup> m<sup>-2</sup> at 10  $\mu$ m.

This indicates that earth-based interstellar communication is favorable for  $\lambda < 2.5 \mu$ m. For telescopes on other planets, we would need to know precisely the exoplanet atmospheres, exozodiacal dust, etc. which may result in a different noise structure; a detailed discussion is beyond the scope of this paper.

#### 4.2. Background light from zodiacal light

Space telescopes are not affected by the strong atmospheric light. However, they still collect undesired photons. The strongest source is sunlight which is scattered off of dust grains in the solar system, an effect called zodiacal light. In the ecliptic plane, it can be as bright as  $1.5 \times 10^{-6}$  ergs s<sup>-1</sup> cm<sup>-2</sup> Å<sup>-1</sup>. It is faintest at heliocentric longitude 130°–170° away from the sun because of larger scattering angles, and at low ecliptic latitudes  $< 30^\circ$  because of the minimum in the interplanetary dust column density at levels  $< 10^{-7}$  ergs s<sup>-1</sup> cm<sup>-2</sup> Å<sup>-1</sup> (Bernstein et al. 2002). The scattering strength only weakly depends on wavelength and closely resembles the solar spectrum between 150 nm and 10  $\mu$ m (Leinert et al. 1981; Matsuura et al. 1995).

These levels contribute a flux of order  $3 \gamma$  nm<sup>-1</sup> arcsec<sup>-2</sup> m<sup>-2</sup> at 1  $\mu$ m in the ecliptic, and decrease to 0.1 (0.03) photons at latitude 45° (90°). We show an all-sky map in Figure 6 which makes it clear that the source’s location on the sky is important, in addition to the wavelength.

#### 4.3. Background light from galactic and extragalactic sources

The Galactic light comes from stars, starlight scattered from interstellar dust, and line emission from

<sup>4</sup> Data files from <http://www.gemini.edu/sciops/telescopes-and-sites/observing-condition-constraints/optical-sky-background>

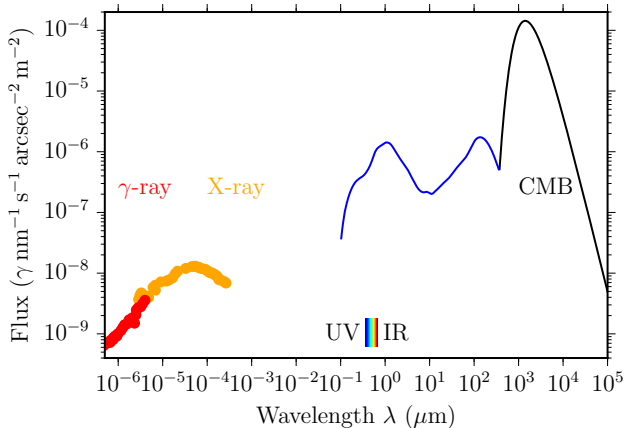


**Figure 7.** Intensity of the extragalactic background after removal of the zodiacal light foreground (which is strongest in the visible and IR). The peak in the optical is from nuclear fusion, the peak in the FIR from re-radiated dust. The UV/soft X-ray background at a wavelength of 10–100 nm is unknown. Data from [Leinert & Mattila \(1998\)](#); [Cooray \(2016\)](#); [Stecker et al. \(2016\)](#).

the warm interstellar medium. Its levels are of order  $10^{-9} \text{ ergs s}^{-1} \text{ cm}^{-2} \text{ \AA}^{-1}$  between 200 nm and  $1 \mu\text{m}$ .

The mean flux of the optical extragalactic background light has been measured as  $4.0 \pm 2.5$ ,  $2.7 \pm 1.4$  and  $2.2 \pm 1.0 \times 10^{-9} \text{ ergs s}^{-1} \text{ cm}^{-2} \text{ \AA}^{-1}$  at wavelengths of 300 nm, 550 nm and 800 nm ([Bernstein et al. 2002](#)).

Compared to the zodiacal light, these sources are weaker by two orders of magnitude and are only relevant if the source is near the ecliptic poles, where zodi is smallest; and for wavelengths outside the zodi-band of  $\approx 0.3 - 300 \mu\text{m}$ .

#### 4.4. Scintillation and scattering of photons

Extinction causes not only a loss of photons from absorption, but also scattering. The latter reduces the “prompt” pulse height and produces an exponential tail ([Howard et al. 2000](#)).

Scatter broadening is well known from pulsars and magnetars. As an extreme example, magnetars close (0.1 pc) to the galactic center with dispersion measures  $\text{DM} = 1778 \text{ pc cm}^{-3}$  have their pulses broadened to  $1.423 \pm 0.32 \text{ s}$  at 1.2 GHz, and  $0.2 \pm 0.07 \text{ ms}$  at 18.95 GHz, following a power law with index  $-2.8$  ([Spitler et al. 2014](#)). A single pulse which is broadened to a width of one second results in a very low data rate of order bit/s. Extrapolating with the power law indicates that nanosecond pulse widths ( $10^{-9} \text{ s}$ ) can be expected for frequencies  $> 500 \text{ GHz}$  ( $\lambda < 0.6 \text{ mm}$ ), and the broadening should become shorter than the wavelength at  $\lambda \approx \mu\text{m}$ .

For these higher frequencies, the amplitude level of the scattering tail, and its length, is unknown in practice. Limits from the Crab pulsar show no detectable scat-

tering tail at UV and optical wavelengths for an optical millisecond pulse width and  $E(B - V) = 0.52$  ([Sollerman et al. 2000](#)), consistent with the power law scaling from radio observations. These results indicate that the impact of extinction is mainly on the absorption for frequencies  $> 500 \text{ GHz}$  ( $< 0.6 \text{ mm}$ ), and not on pulse broadening. Therefore, we neglect this effect in our calculations, but suggest further research in this area.

#### 4.5. Background light from the target star and celestial bodies

On the direct path, even modest-sized telescopes receive a relevant number of photons from nearby stars. For example,  $5 \times 10^{10} \gamma \text{ sec}^{-1} \text{ m}^{-2}$  from  $\alpha \text{ Cen A}$  (distance 1.3 pc, [Kervella et al. 2016](#),  $L = 1.522 L_{\odot}$ ). From Proxima Centauri ( $L = 1.38 \times 10^{-4} L_{\odot}$ ), it is  $4.25 \times 10^6 \gamma \text{ sec}^{-1} \text{ m}^{-2}$ , or  $3.5 \times 10^9 (3.5 \times 10^5) \gamma \text{ sec}^{-1} \text{ m}^{-2}$  from a sun-like star in a distance of 10 LY (1000 LY). A coronagraph or occulter could be used to block a significant part of this flux ( $10^{-9}$ , [Guyon et al. 2006](#); [Liu et al. 2015](#)). Additionally, a filter with a small band-pass, e.g. 1 nm, would reduce the flux further by  $> 10^3$ . A good angular resolution of the receiving telescope would be helpful to separate the transmitter from the nearby target star. For comparison, a probe at a distance of 1 au from the star  $\alpha \text{ Cen A}$  would appear at an angular separation of 1.42 arcsec as seen from earth, resolvable even with small telescopes, assuming sufficient contrast.

The flux levels from reflected exoplanet light and exozodiacal dust is many orders of magnitude fainter than from the flux in the home solar system, and can thus be neglected.

#### 4.6. Instrumental noise

Apart from a loss of photons from imperfect reflection or transmission in the receiver, the conversion from photons to electrons (e.g. with CCDs or photomultiplier tubes, which are analogue devices) causes a small, but nonzero amount of noise.

Even a perfect instrument will produce some noise. Fundamentally, this originates from the fact that photons and electrons are quantized ([Einstein 1905](#)), so that only a finite number can be counted in a given time. This phenomenon is the shot noise ([Schottky 1918](#)), and is correlated with the brightness of the target.

## 5. RESULTS

### 5.1. A Starshot-like probe at $\alpha \text{ Centauri}$

We will now calculate exemplary quantitative data rates. Our default example is to maximize data rates with a probe at  $\alpha \text{ Cen}$  ( $d = 1.3 \text{ pc}$ ) and examine the influence of the variables presented in the previous section. Our standard example probe uses a telescope with a circular aperture  $D_t = 1 \text{ m}$ , through which it transmits with a power of  $P = 1,000 \text{ W}$ . The telescope quality  $Q_R \approx 1.22$  for  $\lambda > 300 \text{ nm}$  is of current (earth

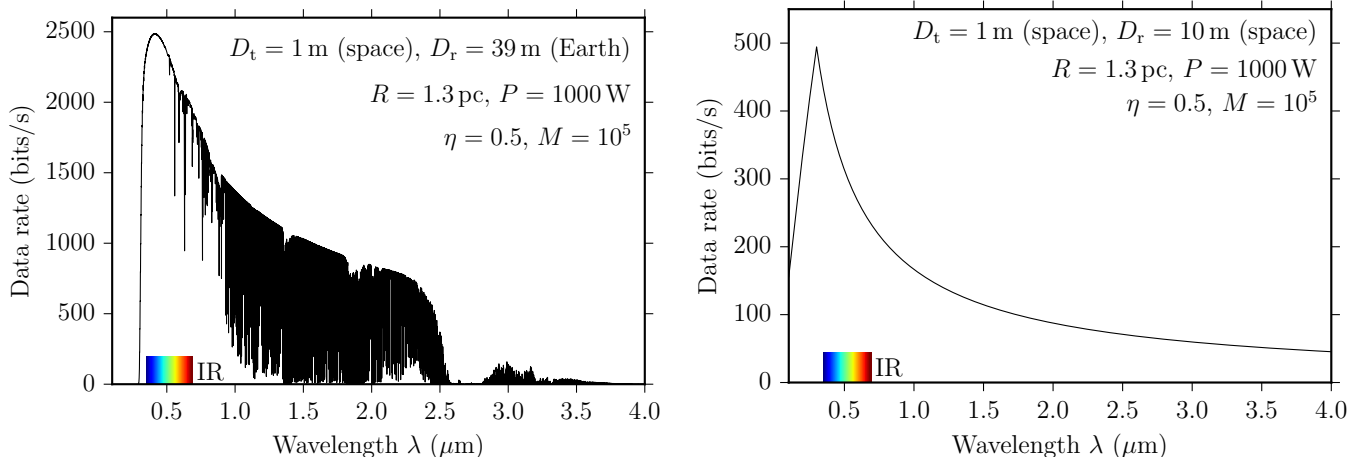


**Figure 8.** Data rate to a probe at Proxima, as a function of wavelength, for the listed parameters. Left: Receiver on earth peaks for  $\lambda = 429.6$  nm. Right: Receiver in space peaks at 300 nm. See text for discussion.

2017) technology, and positioned in space. The hypothetical receiver has  $D_r = 39$  m, comparable to the upcoming generation of “extremely large telescopes” (E-ELTs). It must be located in the southern hemisphere, e.g. in Chile, because  $\alpha$  Cen is not observable from Mauna Kea’s northern latitude which served as an example in previous sections. The total receiver efficiency is  $\eta = 0.5$ . It uses  $N = 10^5$  modes, which could be done with a  $R = 100,000$  spectrograph,  $10^5$  time slots, or a combination of both. The atmospheric sky background represents very good (20-percentile) conditions as described in section 4.1.

From the transmitted  $P = 1,000$  W ( $2.2 \times 10^{21} \gamma s^{-1}$  at  $\lambda = 429.6$  nm), the theoretical flux near earth after free-space loss is  $1,860 \gamma s^{-1}$  in the receiver aperture. Interstellar extinction for this wavelength and distance is  $\approx 0.3\%$ , causing a loss of 6 photons, or a reduction to  $1,854 \gamma s^{-1}$ . Sky transparency is 0.74, so that  $1,369 \gamma s^{-1}$  survive. This is the signal before receiver efficiency.

Regarding the total sky background, we assume that the filter width at the receiver has a bandpass of 1 nm, and the on-sky resolution is 1 arcsec. We neglect the photon flux from  $\alpha$  Cen as it can be effectively suppressed (section 4.5), and is then negligible compared to the atmospheric background of  $0.6 \gamma \text{ nm}^{-1} \text{ s arcsec}^{-2} \text{ m}^{-2}$  (section 3.2), resulting in 702 noise photons per second in the telescope. We will discuss the case of blended sources (probe and star) in section 6.5. We also neglect the noise flux from the receiver itself. Following Eq. 7, the Holevo bound with our noise is then 1.81 bits per photon. This includes the receiver efficiency of  $\eta = 0.5$ .

We can now multiply the received photons with the encoding limit and estimate  $1,369 \gamma s^{-1}$  at  $1.81 \text{ bits } \gamma^{-1} = 2480 \text{ bits/s}$ . This is also the peak value at  $\lambda = 429.6$  nm in Figure 8 (left), indicating that any other wavelength decreases the effective data rate. In practice, this is an

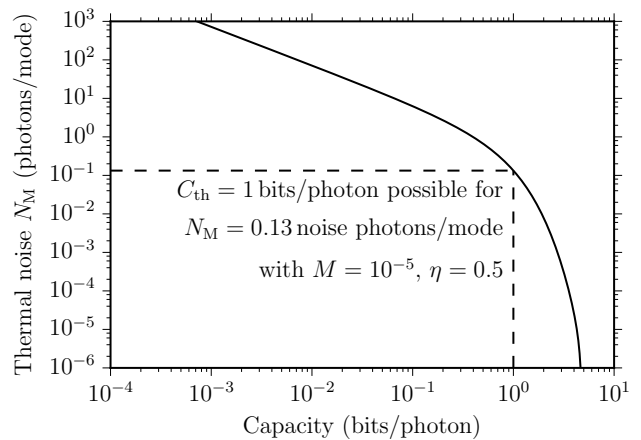


**Figure 9.** Capacity  $C_{th}$  (in bits/photon) is a logarithmic function of thermal noise  $N_M$  (in photons per mode).

upper bound; realistic data rates including sensor noise, margin for error, etc. will yield smaller data rates by a factor of a few.

The cut-off for  $\lambda < 290$  nm comes from the atmospheric intransparency (Figure 3). The decline in data rate towards longer wavelengths comes from two effects: the decrease in telescope focusing (section 3.3), and increasing atmospheric noise (Figure 5). Individual atmospheric absorption lines can be clearly seen which should be avoided for communication (Figures 3, 5).

## 5.2. Space-based receiver

For the space-based analysis, we restrict the receiver size to  $D_r = 10$  m to make it more realistic for the current technological level. The optimal wavelength is now  $\lambda \approx 300$  nm which is limited by the telescope quality (Figure 4). Noise levels are dominated by zodiacal light;  $\alpha$  Cen is  $42^\circ$  from the ecliptic, resulting in noise levels of  $\approx 0.1 \gamma \text{ nm}^{-1} \text{ s arcsec}^{-2} \text{ m}^{-2}$  and a higher capacity of



2.83 bits per photon. The signal decreases to  $174 \gamma^{-1}$  for a maximum data rate of 494 bits/s.

### 5.3. Power

At first approximation, data rate is a linear function of power,  $DSR_\gamma \propto P$ . This holds for constant capacity  $C_{th}$  which however depends on the ratio of signal to noise, and thus decreases for decreasing signal. The effect is small for  $S \gg N$  but becomes very considerable for  $N > S$ . As shown in Figure 9, a capacity  $C_{th} = 1$  bits per photon is possible for  $N_M \leq 0.13$  (noise photons per mode) in our standard example using  $M = 10^{-5}$  modes and receiver efficiency  $\eta = 0.5$ . Capacity is a logarithmic function of SNR, and the sweet spot appears between 0.1–5 bits/photon, which is achievable for  $10^{-6} < N_M < 10$  assuming  $10^5$  modes and  $\eta = 0.5$ .

### 5.4. Transmitter size

The transmitter size for a circular aperture scales as  $DSR_\gamma \propto D_t^2$  assuming no technological limitations, which we identify as possible for current (earth 2017) technology at  $\lambda > 300$  nm. Increasing the dish size to focus optical lasers is thus very beneficial for the data rate, and it is recommended to make the aperture as large and high-quality as possible.

### 5.5. Receiver size

The receiver size for a circular aperture scales as  $DSR_\gamma \propto D_r^2$ , and we here relax the technological limitations: imperfect focusing will still collect all photons (signal), but collect more noise due to the larger beam width; the total effect is however much smaller. For a real application, this additional noise factor can be modeled.

### 5.6. Interstellar Extinction

Extinction is largely irrelevant for the shortest interstellar distances,  $< 1\%$  in the optical to  $\alpha$  Cen. Outside of the Lyman continuum ( $\approx 50 < \lambda < 91.2$  nm), any frequency is equally suitable. The situation changes significantly for distances  $> 200$  pc, where optical extinction is  $> 0.5$  (compare Figure 2). To examine the optimal choice of wavelength versus distance due to extinction, we have plotted the normalized photon rate in Figure 10, and subtracted out the free-space loss. The optimal wavelength for space-based communication is limited by technology at 300 nm out to 200 pc, and increases to  $3 \mu\text{m}$  for the longest paths in the galaxy. For an earth-based receiver, the lower limit is 420 nm due to limited atmospheric transmission, and special care must be taken not to select a narrow absorption line.

In this calculation, we assumed uniform extinction of  $A(V) = 1.8$  mag per kpc in the galactic plane (Whittet 2003). In reality, however, the situation is much more complex. Extinction in the galactic plane can vary on small scales (because of individual molecular clouds),

and on large (degree) scales (Schlafly et al. 2016). Galactic communication with maximized data rates will require a precise measurement along each line of sight (communication path) to choose the best wavelength. If a civilization, or a club of civilizations, prefers to choose a single frequency for all distances, it will be at  $\approx 3 \mu\text{m}$ . Then, long distance communication is near optimal (it would be prohibitive at shorter wavelengths), while data rates for short-distance communication are smaller by a factor of a few compared to individual optima.

## 6. DISCUSSION

### 6.1. Assessment of achievable data rates

Achievable data rates are of order kbits/s per KW for a meter-sized probe at  $\alpha$  Cen. For comparison, the NASA probe “New Horizons” achieved a data rate of 1 kbits/s at  $P = 13$  W from Pluto, and transmitted a total of 50 Gbits ( $5 \times 10^{10}$  bits, buffered) over the course of 15 months. The transfer of an image as shown in Figure 11 with a compressed volume of  $\approx 400$  kbits takes 7 min to transfer at 1 kbits/s for a  $P = 1$  kW at  $\alpha$  Cen, or days (to weeks with problematic SNR) at  $P = 1$  W, which might be regarded as acceptable.

Photovoltaic energy is available at a level of  $\text{kW m}^{-2}$  at au distance from the star, so that a probe in orbit (perhaps decelerated by stellar photons, Heller & Hippke (2017); Heller et al. (2017)) has no power issues for transmissions. A fly-by probe at 20% c, however, transverses the au distance in 17 minutes, translating into a data volume of order  $\text{Mbits m}^{-2}$  if the whole time were used for transmission (which is unrealistic, given that the target exoplanet is to be observed). Available photovoltaic energy decreases with the inverse square to the distance from the star, and by integrating over an exemplary trajectory with a closest encounter of 1 au to the star we can estimate the total collected photovoltaic energy, during the fly-by, of order  $\text{kWh m}^{-2}$ . With this energy, perhaps stored on-board and used for later transmission, the probe can send a few  $\text{Mbits m}^{-2}$ , i.e. a few high-quality images (Figure 11). Alternative options would require an onboard energy source.

### 6.2. Onboard storage requirements

The data volume during the fly-by governs the size of the transmission buffer. “New Horizons” carried a total of 16 GBs, which contained all the data it recorded during the fly-by, and which was transferred afterwards. The same scheme could be used for a fly-by at  $\alpha$  Cen. If the probe starts to transmit after the observations, and transmits 1 bit/s (1 kbit/s) for a total of 10 years remaining lifetime, it can transfer (and needs to store) a total of 31 Mbits (31 Gbits). Both are low numbers and can be stored with current (Earth 2017) technology at millimeter sizes and milligram masses.

### 6.3. Earth’s rotation

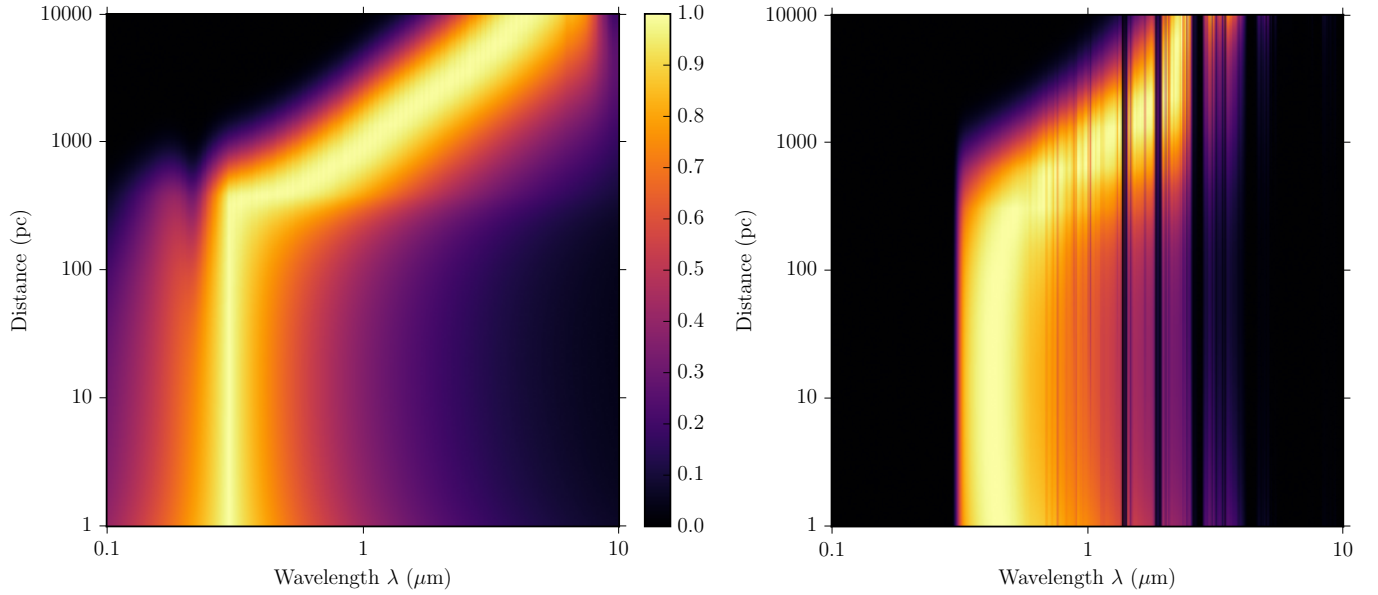


**Figure 10.** Best frequency (brightest color) as a function of distance. The influence of free space loss has been subtracted out as it would have overpowered all other parameters. Left: Space-based telescope. Right: earth-based, including atmospheric transmission. The optimal wavelength is close to  $0.3 \mu\text{m}$  for distances  $< 200 \text{ pc}$  and increases to the mid-IR for larger distances.

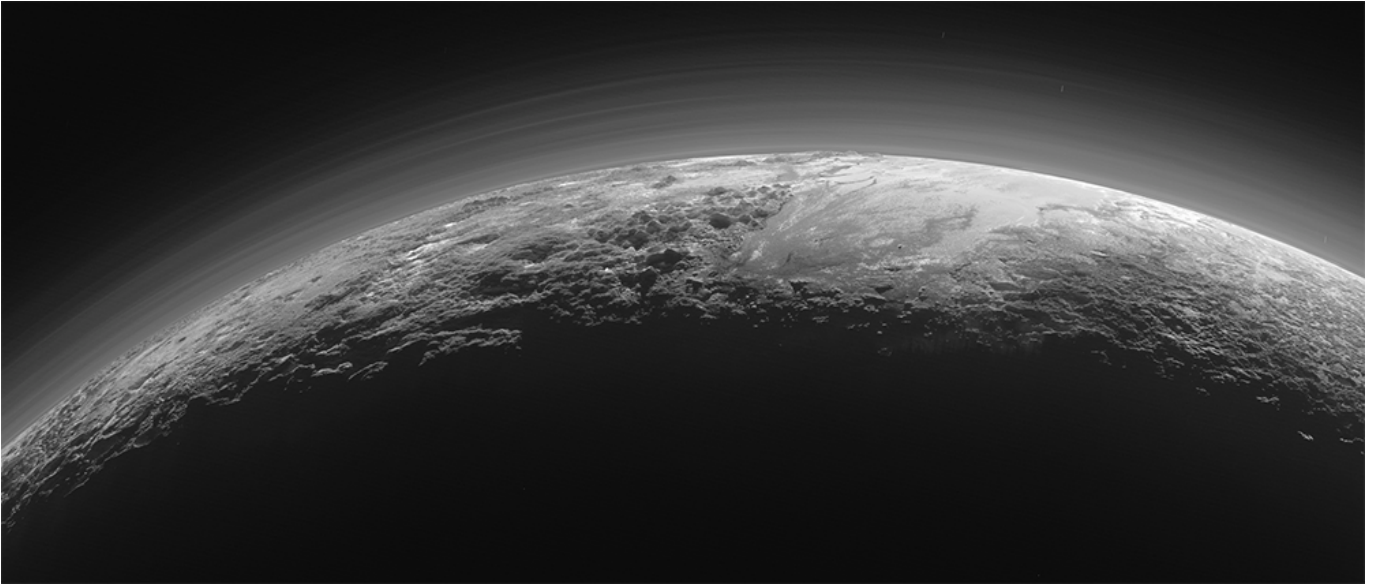


**Figure 11.** Pluto image taken by “New Horizons” with a compressed (lossy) data volume of  $\approx 400 \text{ kbits}$  for the shown quality.

A space-based receiver, for example at a Lagrangian point, can be used near-continuously. Earth-based telescopes, however, suffer from Earth’s rotation (daylight) and weather. When “New Horizons” encountered Pluto, the entire NASA Deep Space Network was online to ensure there were no breaks in reception. If the communication scheme with  $\alpha \text{ Cen}$  is the same, a large number of telescopes will be required. We can, however, replace (expensive) 39 m E-ELTs with a number of smaller telescopes. To replace one E-ELT in terms of aperture,

$\approx 1,500$  telescopes with  $d = 1 \text{ m}$  are required, or 24 telescopes with  $d = 8 \text{ m}$ .

#### 6.4. Laser line width, orbital motion, beam sizes

Transmitter and receiver are in relative motion, which results in a change of path length, as already noted by Messerschmitt (2013, 2015). If the sender (receiver) is located on a planet which orbits a star, the Doppler shift will cause a shift in the sender (receiver) frequency. For example, earth’s equatorial speed is  $465.1 \text{ m/s}$ , or a frequency shift of  $1.55 \times 10^{-6}$ . This is an order of magni-

tude smaller than current spectrographs ( $R = 100,000$ ), but larger than typical high-power laser line-widths (350 MHz, or  $6 \times 10^{-6}$ , Duarte (1999)) by a factor of a few. Laser line width in the mHz range, although at low ( $10^{-12}$  W) power, have been demonstrated (Meiser et al. 2009; Kessler et al. 2012). For such small line widths, the shift would need to be modeled and compensated. Regarding noise per mode (atmospheric, zodiacal etc.), very narrow line widths are preferred.

Narrow line widths may give rise to additional noise sources, namely instrumental frequency shifts in the sender and/or receiver, or a change in the interstellar scattering geometry, which may also result in non-gaussian noise per sub-channel.

For the closest stars within a few pc, large optical telescopes (10-100 m) have diffraction-limited (adaptive optics) beam sizes smaller than typical orbits (au) of exoplanets. When using such tight beams in the transmitter, the position of the receiving telescope (e.g. on a planet in motion) needs to be known with high accuracy at the time of arrival of the photons (Sherwood et al. 1992; Mankevich & Orlov 2016).

### 6.5. Blend of probe and star

In the previous sections, we have neglected the noise flux from the target star. This is justified for sky-projected separations which allow for the use of coronagraphs, and suppress  $10^{-9}$  (Guyon et al. 2006; Liu et al. 2015) of the starlight ( $4.25 \times 10^6 \gamma \text{sec}^{-1} \text{m}^{-2}$ ) at a separation of 1 au at Proxima Centauri. During most of the flight, the problem is much less severe because of the large proper motion of  $\alpha$  Cen ( $3.7 \text{arcsec} \text{yr}^{-1}$ , Kervella et al. 2016).

We can estimate data rates for this increased noise level within the Holevo bound for this situation, and get a capacity of order  $10^{-5}$  bits per second per Watt. Such a low data rate is insufficient for the transfer of images or other observational data, but may be sufficient for simple telemetry and onboard health status.

### 6.6. Current technological level and photon dimensions

The Holevo bound assumes the use of a number of modes to encode information into photons. The available modes in photons are their time of arrival (sometimes called phase modulation), their frequency (or color), and their polarization. Realizing  $10^{-5}$  photons per mode will require many ( $> 10^5$ ) modes to encode the information. This can be done with a combination of color, timing and polarization. Commonly used are time-frequency modulations. The usage of polarized light is less common, but might be beneficial for our case. Starlight is polarized only by a few percent (Foshiba et al. 2002), so that the use of polarization, which is possible for lasers, can reduce noise levels by a factor of two.

We now examine currently available technology. For the sender, the shortest possible laser pulse length has

decreased by 11 orders of magnitude during the last 50 years, from  $100 \mu\text{s}$  in the free-running laser of Maiman (1960) to 67 attoseconds ( $10^{-18}$  s, Zhao et al. 2012). For a detailed history of the exponential improvements, see Agostini & Di Mauro (2004). While the pulse length is very short, the repetition rate is slower by many orders of magnitude.

The highest data rates are currently found in fiber-optic communication by sending pulses of light through an optical fiber, with a current record of order Tbits/s ( $10^{12}$  bits/s) on one glass fiber (Maher et al. 2016). Commercial products are available with data rates 1–3 orders of magnitude below this value. The industry standard employs 100 channels with a channel spacing of 100 GHz (0.8 nm) between 1530 – 1612 nm with a typical bandwidth (frequency range) of 186 – 196 THz (International Telecommunication Union 2012). Limiting factors are small bandwidth (82 nm, or  $b = 5\%$ ), the wavelength stability of lasers with thermal changes, signal degradation from nonlinear effects in optical fibers, inter-channel crosstalk and (clock) timing jitter.

On the receiver side, current photon-counting detectors can be relatively fast (timings below  $10^{-10}$  s) and efficient ( $> 90\%$ ) with a low dark count rate ( $< 1$  c.p.s.), but suffer from longer ( $10^{-7}$  s) reset times (Marsili et al. 2013). Classical photomultiplier tubes offer timings (and reset times) of  $10^{-9}$  s (Dolgoshein et al. 2006). Current photon detectors are fast enough to sample 10 GHz frequencies at the Nyquist limit ( $B < f/2$ , Nyquist 1928). These limits, however, are technological, and further improvements can be expected. The ideal instrument for high-mode communication would be a high-throughput, high-resolution spectrograph with low-noise, high-speed photon counters on each sub-channel.

### 6.7. Bi-directional communication

The focus in this paper was the communication from a distant, small, power-limited probe towards home-base. The opposite way, perhaps to send new instructions, is comparably easier: Home-base has less stringent limits on aperture size and power. Telescope diameters might be larger by 1–2 orders of magnitude, and power by several orders of magnitude. A major issue might be that the probe needs to “listen” at the moment the photons arrive, and not spend the time sending, making observations, or in hibernation. A simple solution would be pre-arranged timeslots.

### 6.8. Comparison to the literature

In his “Roadmap to Interstellar Flight”, Lubin (2016) recently approximated the communication flux as (his section 5.6, our notation)  $F = D^2 P / (4d^2 \lambda^2)$  which yields an overestimate by  $\approx 11.7\%$  compared to our Eq. 2.

In their “Search for nanosecond optical pulses”, Howard et al. (2000) and Howard et al. (2004) describe

the received photon flux as

$$N_d = \frac{\pi^2 D^2 D^2 E_p}{16 \lambda d^2 h c} \quad (9)$$

(their Eq. 2, neglecting extinction; they set  $D = D_r = D_t$ ). Numerically, this produces a received photon flux which is too high by  $\approx 3.67\times$ .

In their ‘‘Search for Optical Laser Emission’’, [Tellis & Marcy \(2015\)](#) define the received photon flux in the same form as in our Eq. 2 (their Eq. 5), but with an incorrect divisor of 2, resulting in  $4\times$  too many photons received.

The work by [Horwath \(1996\)](#) discusses beam widths and frequencies of interstellar laser communications, but neglects extinction, and consequently proposes laser communication in the Lyman H $\alpha$  line at 126 nm over distances of 3,000 LY, which is impossible because of very high UV extinction (Figure 2).

A more traditional interstellar radio communication design from  $\alpha$  Cen has recently been published by [Milne et al. \(2016\)](#). It presents scenarios for antennas with sizes of 1–15 km on both sides, transmitting MW power at 32 GHz, achieving a data rate of Gbits/s ( $10^9$  bits/s). The antenna weight is mentioned as 40,000 kg, and the total space-ship weight is  $10^7$  kg. Clearly, if such masses and power can be sent to other stars, the question of communication will be trivial in comparison.

### 6.9. *PyCom software package*

We provide the Python-based software package `PyCom` as open source under the free MIT license<sup>5</sup>. The repository provides function calls for the equations in this paper, a tutorial, and scripts to reproduce all figures.

## 7. CONCLUSION

In this work (paper I of the series), we have set the framework of data transfer between telescopes, using the

example of a light-weight, power-limited probe at  $\alpha$  Cen. We have explored limiting factors such as extinction, noise, and technological constraints. We have calculated optimal frequencies and achievable data rates.

The Holevo bound gives an upper limit of a few bits per photon for realistic signal and noise levels from a communication between a meter-sized probe at  $\alpha$  Cen and a large (39 m) telescope on earth. The achievable data rate is of order bits per second per Watt. For a probe with a size of a few meters, and photovoltaic energy of  $\text{KW m}^{-2}$ , power levels might be KW, resulting in data rates of order kbits/s. The optimal wavelength for a communication with  $\alpha$  Cen, at current technological levels, is 300 nm (space-based receiver) to 400 nm (earth-based) and increases with distance, due to extinction, to a maximum of  $\approx 3 \mu\text{m}$  to the center of the galaxy at 8 kpc.

A critical requirement in this scheme is the coronagraphic suppression of the stellar background at the level of  $10^{-9}$  within a few tenths of an arcsecond of the bright star, which has not been demonstrated yet. Further research on this topic is encouraged.

In paper II, the use of a stellar gravitational lens will be discussed. In paper III, we will relax technological constraints to explore the ultimate, most efficient interstellar communication scheme which yields insight into communication of more advanced life in the universe, if it exists.

The author is thankful to René Heller, Duncan Forgan, John Learned and Tony Zee for helpful discussions, and to the Breakthrough Initiatives for an invitation to the Breakthrough Discuss 2017 conference at Stanford University.

## REFERENCES

- Agostini, P., & Di Mauro, L. F. 2004, [Reports on Progress in Physics](#), **67**, 813
- Aller, L. H. 1959, [PASP](#), **71**, 324
- Aristov, V. V., & Shabel’nikov, L. G. 2008, [Physics Uspekhi](#), **51**, 57
- Barstow, M. A., & Holberg, J. B. 2007, *Extreme Ultraviolet Astronomy*
- Bekenstein, J. D. 1981, [PhRvD](#), **23**, 287
- Bernstein, R. A., Freedman, W. L., & Madore, B. F. 2002, [ApJ](#), **571**, 56
- Boggess, N. W., Mather, J. C., Weiss, R., et al. 1992, [ApJ](#), **397**, 420
- Bond, A., & Martin, A. R. 1978, *Journal of the British Interplanetary Society*, **31**, S5
- Bradley, J., Dai, Z. R., Erni, R., et al. 2005, [Science](#), **307**, 244
- Burrows, D. N., Hill, J. E., Nousek, J. A., et al. 2005, [SSRv](#), **120**, 165
- Canfield, D. E., Poulton, S. W., & Narbonne, G. M. 2007, [Science](#), **315**, 92
- Chitode, J. 2009, *Communication Theory (Technical Publication)*
- Cooray, A. 2016, [Royal Society Open Science](#), **3**, 150555

<sup>5</sup> <http://github.com/hippke/communication/>

- Coulman, C. E., Vernin, J., & Fuchs, A. 1995, *ApOpt*, **34**, 5461
- Danjon, A., & Couder, A. 1935, Lunettes et telescopes - Theorie, conditions d'emploi, description, reglage
- Dias, W. S., Alessi, B. S., Moitinho, A., & Lépine, J. R. D. 2002, *A&A*, **389**, 871
- Dolgoshein, B., Balagura, V., Buzhan, P., et al. 2006, *Nuclear Instruments and Methods in Physics Research A*, **563**, 368
- Draine, B. T. 2003a, *ARA&A*, **41**, 241
- . 2003b, *ApJ*, **598**, 1017
- . 2003c, *ApJ*, **598**, 1026
- Duarte, F. 2015, *Tunable Laser Optics*, Second Edition (CRC Press)
- Duarte, F. J. 1999, *ApOpt*, **38**, 6347
- Dyson, F. J. 1965, *Science*, **149**, 141
- . 1968, *Physics Today*, **21**, 41
- Einstein, A. 1905, *Annalen der Physik*, **322**, 132
- Forbes, J. D. 1842, *Philosophical Transactions of the Royal Society of London Series I*, **132**, 225
- Fosalba, P., Lazarian, A., Prunet, S., & Tauber, J. A. 2002, in *American Institute of Physics Conference Series*, Vol. 609, *Astrophysical Polarized Backgrounds*, ed. S. Cecchini, S. Cortiglioni, R. Sault, & C. Sbarra, 44
- Fritz, T. K., Gillessen, S., Dodds-Eden, K., et al. 2011, *ApJ*, **737**, 73
- Giovannetti, V., García-Patrón, R., Cerf, N. J., & Holevo, A. S. 2014, *Nature Photonics*, **8**, 796
- Giovannetti, V., Guha, S., Lloyd, S., Maccone, L., & Shapiro, J. H. 2004a, *PhRvA*, **70**, 032315
- Giovannetti, V., Guha, S., Lloyd, S., et al. 2004b, *Physical Review Letters*, **92**, 027902
- Gorenstein, P. 2004, in *Proc. SPIE*, Vol. 5168, *Optics for EUV, X-Ray, and Gamma-Ray Astronomy*, ed. O. Citterio & S. L. O'Dell, 411
- Guha, S., & Wilde, M. M. 2012, ArXiv e-prints, [arXiv:1202.0533 \[cs.IT\]](https://arxiv.org/abs/1202.0533)
- Guharay, A., Nath, D., Pant, P., et al. 2009, *Journal of Geophysical Research (Atmospheres)*, **114**, D18105
- Guyon, O., Pluzhnik, E. A., Kuchner, M. J., Collins, B., & Ridgway, S. T. 2006, *ApJS*, **167**, 81
- Hardy, J. W. 1998, *Adaptive Optics for Astronomical Telescopes*, 448
- Heller, R., & Hippke, M. 2017, *ApJL*, **835**, L32
- Heller, R., Hippke, M., & Kervella, P. 2017, ArXiv e-prints, [arXiv:1704.03871 \[astro-ph.IM\]](https://arxiv.org/abs/1704.03871)
- Holevo, A. S. 1973, *Problemy Peredachi Informatsii*, **9**, 3
- Horwath, J. S. 1996, in *Proc. SPIE*, Vol. 2704, *The Search for Extraterrestrial Intelligence (SETI) in the Optical Spectrum II*, ed. S. A. Kingsley & G. A. Lemarchand, 61
- Howard, A., Horowitz, P., Coldwell, C., et al. 2000, in *Astronomical Society of the Pacific Conference Series*, Vol. 213, *Bioastronomy 99*, ed. G. Lemarchand & K. Meech
- Howard, A. W., Horowitz, P., Wilkinson, D. T., et al. 2004, *ApJ*, **613**, 1270
- International Telecommunication Union. 2012, *Increasing the information rates of optical communications via coded modulation: a study of transceiver performance* (<http://www.itu.int/rec/T-REC-G.694.1-201202-I/en>)
- Jones, H. W. 1995, in *Astronomical Society of the Pacific Conference Series*, Vol. 74, *Progress in the Search for Extraterrestrial Life.*, ed. G. S. Shostak, 369
- Kaushal, H., Jain, V., & Kar, S. 2017, *Free Space Optical Communication*, *Optical Networks* (Springer India)
- Kelsall, T., Weiland, J. L., Franz, B. A., et al. 1998, *ApJ*, **508**, 44
- Kepler, J. 1604, *De cometis liballi tres* (Frankfurt, Germany)
- Kervella, P., Mignard, F., Mérand, A., & Thévenin, F. 2016, *A&A*, **594**, A107
- Kessler, T., Hagemann, C., Grebing, C., et al. 2012, *Nature Photonics*, **6**, 687
- Klein, B. J., & Degnan, J. J. 1974, *ApOpt*, **13**, 2134
- Kuiper, G. P. 1950, *PASP*, **62**, 133
- Leinert, C., & Mattila, K. 1998, in *Astronomical Society of the Pacific Conference Series*, Vol. 139, *Preserving The Astronomical Windows*, ed. S. Isobe & T. Hirayama, 17
- Leinert, C., Richter, I., Pitz, E., & Planck, B. 1981, *A&A*, **103**, 177
- Levasseur-Regourd, A. C., & Dumont, R. 1980, *A&A*, **84**, 277
- Liu, C.-C., Ren, D.-Q., Dou, J.-P., et al. 2015, *Research in Astronomy and Astrophysics*, **15**, 453
- Lord, S. D. 1992, *A new software tool for computing Earth's atmospheric transmission of near- and far-infrared radiation*, Tech. rep.
- Lubin, P. 2016, ArXiv e-prints, [arXiv:1604.01356 \[astro-ph.EP\]](https://arxiv.org/abs/1604.01356)
- Maher, R., Alvarado, A., Lavery, D., & Bayvel, P. 2016, *Scientific Reports*, **6**, 21278
- Maihara, T., Iwamuro, F., Yamashita, T., et al. 1993, *PASP*, **105**, 940
- Maiman, T. H. 1960, *Nature*, **187**, 493
- Mankevich, S. K., & Orlov, E. P. 2016, *Quantum Electronics*, **46**, 966
- Marshall, W. K. 1987, *ApOpt*, **26**, 2055
- Marsili, F., Verma, V. B., Stern, J. A., et al. 2013, *Nature Photonics*, **7**, 210

- Matsuura, S., Matsumoto, T., Matsuhara, H., & Noda, M. 1995, *Icarus*, **115**, 199
- Maxwell, J. C. 1873, *A Treatise on electricity and magnetism*, Vol. 2 (Macmillan & Co., London)
- Maxwell, J. C., & Harman, P. M. 1990, *The Scientific Letters and Papers of James Clerk Maxwell: 1846-1862*, *The Scientific Letters and Papers of James Clerk Maxwell* (Cambridge University Press)
- McJunkin, M., France, K., Schindhelm, E., et al. 2016, *ApJ*, **828**, 69
- Meiser, D., Ye, J., Carlson, D. R., & Holland, M. J. 2009, *Physical Review Letters*, **102**, 163601
- Messerschmitt, D. G. 2013, ArXiv e-prints, [arXiv:1305.4684](https://arxiv.org/abs/1305.4684) [[astro-ph.IM](https://arxiv.org/abs/1305.4684)]
- . 2015, *Acta Astronautica*, **107**, 20
- Milne, P., Lamontagne, M., & Freeland, R. 2016, *Journal of the British Interplanetary Society*, **69**, 278
- Nyquist, H. 1928, *Transactions of the American Institute of Electrical Engineers*, Volume 47, Issue 2, pp. 617-624, **47**, 617
- Plastino, A. R., & Muzzio, J. C. 1992, *Celestial Mechanics and Dynamical Astronomy*, **53**, 227
- Popkin, G. 2017, *Nature*, **542**, 20
- Porquet, D., Grosso, N., Predehl, P., et al. 2008, *A&A*, **488**, 549
- Poudel, A., McDermott, R., & Vavilov, M. G. 2012, *PhRvB*, **86**, 174506
- Rayleigh, L. 1879, *Philosophical Magazine Series 5*, **8**, 261
- Redding, J. L. 1967, *Nature*, **213**, 588
- Ryter, C. E. 1996, *Ap&SS*, **236**, 285
- Salmaso, B., Basso, S., Brizzolari, C., et al. 2014, in *Proc. SPIE*, Vol. 9151, *Advances in Optical and Mechanical Technologies for Telescopes and Instrumentation*, 91512W
- Schlafly, E. F., Meisner, A. M., Stutz, A. M., et al. 2016, *ApJ*, **821**, 78
- Schottky, W. 1918, *Annalen der Physik*, **362**, 541
- Shannon, C. E. 1949, *Proc. Institute of Radio Engineers*, **37**, 10
- Sherwood, B., Mumma, M. J., & Donaldson, B. K. 1992, in *Lunar Bases and Space Activities of the 21st Century*, ed. W. W. Mendell, J. W. Alred, L. S. Bell, M. J. Cintala, T. M. Crabb, R. H. Durrett, B. R. Finney, H. A. Franklin, J. R. French, & J. S. Greenberg
- Smith, M. G., Warner, M., Orellana, D., et al. 2008, in *Astronomical Society of the Pacific Conference Series*, Vol. 400, *Preparing for the 2009 International Year of Astronomy: A Hands-On Symposium*, ed. M. G. Gibbs, J. Barnes, J. G. Manning, & B. Partridge, 152
- Sollerman, J., Lundqvist, P., Lindler, D., et al. 2000, *ApJ*, **537**, 861
- Spitler, L. G., Lee, K. J., Eatough, R. P., et al. 2014, *ApJL*, **780**, L3
- Stecher, T. P. 1965, *ApJ*, **142**, 1683
- . 1969, *ApJL*, **157**, L125
- Stecker, F. W., Scully, S. T., & Malkan, M. A. 2016, *ApJ*, **827**, 6
- Takeoka, M., & Guha, S. 2014, *PhRvA*, **89**, 042309
- Tanguay, J., Yun, S., Kim, H. K., & Cunningham, I. A. 2013, *Medical Physics*, **40**, 041913
- . 2015, *Medical Physics*, **42**, 491
- Tellis, N. K., & Marcy, G. W. 2015, *PASP*, **127**, 540
- Tinsley, J. N., Molodtsov, M. I., Prevedel, R., et al. 2016, *Nature Communications*, **7**, 12172
- Valencic, L. A., Clayton, G. C., & Gordon, K. D. 2004, *ApJ*, **616**, 912
- Vergely, J.-L., Ferrero, R. F., Egret, D., & Koeppen, J. 1998, *A&A*, **340**, 543
- Whittet, D. C. B., ed. 2003, *Dust in the galactic environment*
- Wilde, M. M., Guha, S., Tan, S.-H., & Lloyd, S. 2012, ArXiv e-prints, [arXiv:1202.0518](https://arxiv.org/abs/1202.0518) [[quant-ph](https://arxiv.org/abs/1202.0518)]
- Wilms, J., Allen, A., & McCray, R. 2000, *ApJ*, **542**, 914
- Wong, C. H., & Vavilov, M. G. 2015, ArXiv e-prints, [arXiv:1512.06939](https://arxiv.org/abs/1512.06939) [[cond-mat.mes-hall](https://arxiv.org/abs/1512.06939)]
- Yuen, H. P., & Shapiro, J. H. 1978, *IEEE Transactions on Information Theory*, **24**, 657
- Zhao, K., Zhang, Q., Chini, M., et al. 2012, *Optics Letters*, **37**, 3891